ELSEVIER

International Journal of Heat and Fluid Flow 23 (2002) 22–28

International Journal of HEAT AND FLUID FLOW

www.elsevier.com/locate/ijhff

Jet impingement heat transfer on dimpled target surfaces

Srinath V. Ekkad *, David Kontrovitz

Mechanical Engineering Department, Louisiana State University, Baton Rouge, LA 70803, USA

Received 8 December 2000; accepted 13 September 2001

Abstract

Detailed heat transfer distributions are presented over a jet impingement target surface with dimples. Jet impingement by itself is an extremely effective heat transfer enhancement technique. This study investigates the effect of jet impingement on a target surface with a dimple pattern. The effect of dimple location, underneath the jets or between the jets, is investigated. The effect of dimple depth is also investigated. The average jet Reynolds number is varied from 4800 to 14 800. The heat transfer measurements are obtained using the transient liquid crystal technique. Results for dimpled target surfaces are normalized with data for plane target surfaces to determine whether the presence of dimples enhances heat transfer. Results show that the presence of dimples on the target surface, in-line or staggered with respect to jet location, produce lower heat transfer coefficients than the non-dimpled target surface. The bursting phenomena associated with flow over dimples produces disturbances of the impingement jet structures resulting in lower levels of heat transfer coefficients on the target surface.

Keywords: Impingement; Dimples; Enhancement; Cooling

1. Introduction

Effective cooling techniques are important for maintaining gas turbine component temperature under operable levels. Heat transfer enhancement methods are successfully used inside airfoil internal cooling passages to remove heat from the exposed metal surfaces. Jet impingement is one such popular technique. To further increase the levels of heat transfer enhancement, the surfaces are modified to include pin fins or cavities. In this study, the target surface has dimples machined on the surface. It is expected that adding dimples to the target surface that has jets impinging on it will further enhance heat transfer. Surface dimples are expected to affect the jet impingement structures and promote turbulent mixing and thus enhance heat transfer. This is the first study to deal with impingement over dimpled target surfaces.

Experimental studies of impingement surface heat transfer for gas turbine applications were reported by Chupp et al. (1969), Kercher and Tabakoff (1970), Florschuetz et al. (1981, 1984), and Behbahani and Goldstein (1983). Downs and James (1987) summarized findings relating to parametric effects of geometry, temperature, interference and cross-flow, turbulence levels, surface curvature, and non-uniformity of jet array on jet impingement heat and mass transfer. Viskanta (1993), and Huber and Viskanta (1994a,b) pointed out many different factors that influence heat transfer in multiple jet impingement systems such as: wall–jet interaction, separation distance, jet–jet spacing and diameter, cross-flow or exit of spent air, the orifice arrangement in-line or staggered and target surface condition.

Van Treuren et al. (1994) studied impingement heat transfer under in-line and staggered arrays of jets using a transient liquid crystal technique. They measured both local heat transfer coefficient and adiabatic wall temperature under the impingement jets. However, they studied the effect of cross-flow in only one direction. Huang et al. (1998) presented results for impinging orthogonal jets on a flat target surface with three different exit-flow orientations. They confirmed that the heat transfer distributions on the target surface are significantly affected by cross-flow direction. Cross-flow effects are minimal when the flow exits toward both directions after impingement. Results were correlated for all three

* Corresponding author. Tel.: +1-225-388-5901; fax: +1-225-388-5924.

E-mail address: ekkad@me.lsu.edu (S.V. Ekkad).

0142-727X/02/$ - see front matter
PII: S0142-727X(01)00139-4

Nomenclature

A	heat transfer surface area for flat surface
A_0	heat transfer surface area for dimpled surface
d	dimple depth
D	impingement jet hole diameter
D_d	dimple diameter
H	distance between the impingement plate and the target plate
h	local convection heat transfer coefficient (W/m^2 K)
k	thermal conductivity of acrylic material
k_{air}	thermal conductivity of air
$\dot{m}_c$	cross-flow mass flow rate
$\dot{m}_j$	jet mass flow rate
Nu	Nusselt number on a dimpled surface, hD/k_{air}
Nu_0	Nusselt number on a non-dimpled surface
Pr	Prandtl number
Re_j	average jet Reynolds number, $\rho V_j D/\mu$
s	jet–jet spacing
t	time of liquid crystal color change
T_i	initial temperature of test section
T_g	color change temperature of the liquid crystal (red–green)
T_m	mainstream temperature of the flow
V_j	average jet velocity
X	axial distance on the target surface
Y	spanwise distance on the target surface
α	thermal diffusivity of test section
μ	fluid dynamic viscosity
τ	time-step

exit directions with the jet Reynolds number as parameter. The present study uses the same test setup used by Huang et al. (1998). However, the target surface is replaced with a new target surface with dimples in this study.

Schukin et al. (1995) reported the use of concavities to enhance convective heat transfer. They reported from their findings that concavities provide high heat transfer augmentation at considerably low-pressure drop. Chyu et al. (1997) used concavities or dimples on a surface with channel flow. They used hemispherical and tear-drop type dimples on their surface. Both the geometries provided heat transfer augmentation of around 2.5 over a smooth channel flow case. They also observed that the drag reduction associated with dimples was one half of that observed for ribs or protrusions. Recently, Moon et al. (1999) studied the effect of channel height on the heat transfer augmentation associated with flow over a dimpled surface. They concluded that heat transfer enhancement occurred mostly outside the dimples. Their results also show high thermal performance values for the dimpled surfaces. Lin et al. (1999) performed computations to investigate the mechanisms associated flow over rows of dimples in a channel. They indicated that different dimple patterns provide different flow structures. Also, they indicated that each subsequent dimple produces different types of flow behavior in a row of dimples.

The present study investigates the heat transfer aspects of a jet impingement target surface with dimple patterns. All the previous studies reported for surfaces with dimples were focused on channel flows. Two different dimple patterns, in-line and staggered, are compared for two different dimple depths. The jet average Reynolds number is varied from 4800 to 14 800. Detailed heat transfer distributions on the target surface are measured using the transient liquid crystal technique.

2. Experimental setup and procedure

A detailed description of the test setup and instrumentation is provided by Huang et al. (1998). Fig. 1 presents a schematic of the experimental setup. The experimental setup consists of an image processing system (Panasonic RGB Color CCD Camera, IC-PCI Color Frame Grabber Card, PC and Imaging Software Optimas v.6.2), temperature measurement system, flow loop, and the test section. The RGB camera is focused on the test section and the color FG card is programmed through the software to analyze real-time images for color signals during a transient heat transfer test.

The flow circuit consists of an air supply from a 300-psi compressor. The air is regulated and metered through a standard orifice meter to measure the flow

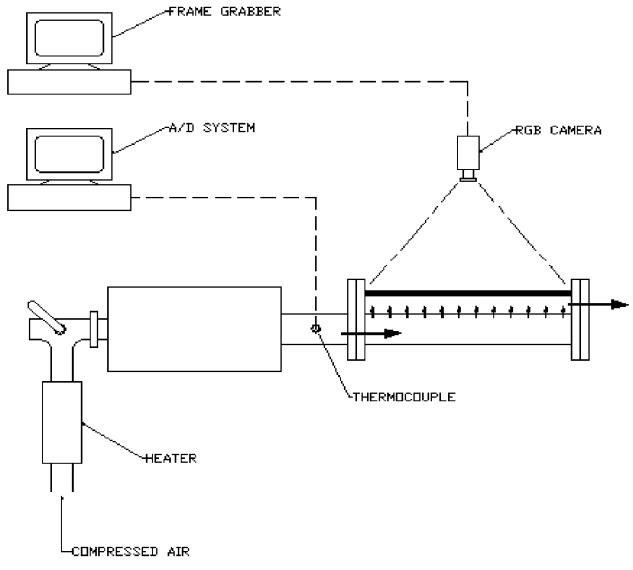

Fig. 1. Experimental setup.

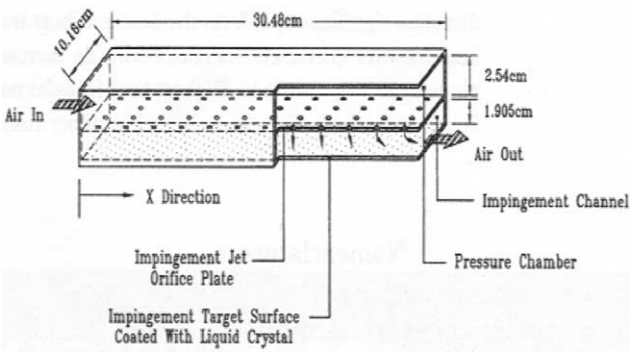

Fig. 2. Illustration of the impingement test section.

rate through the test section. The air is then routed through an in-line air heater (Hotwatt-3 KW) controlled by a temperature controller (CAL3600) system. The air from the heater is then diverted away from the test section with a three-way ball diverter valve. The temperature control unit monitors the heated air temperature by measuring the heated air temperature immediately downstream of the heater. When the valve is flipped, the air is routed through the test section. A series of honeycomb strips and a mesh help produce a uniform flow at the entrance into the test section.

Fig. 2 shows a schematic of the test section. There are 48 impingement holes of 0.635 cm diameter arranged in an array of 12 columns and 4 rows. The jet-to-jet spacing (S/D) is 4-hole diameters. The jet plate to target plate spacing (H/D) is 3-hole diameters. The flow enters the pressure plenum through a narrow channel and exit through the impingement holes and impinges on the target surface. The impingement target surface is coated with a thin layer of thermochromic liquid crystals and black background paint coating. Fig. 3 shows the two dimple patterns on the target plate. The arrows show the location of the impingement jets assuming no cross-flow effects. In the first figure, the jets impinge directly into the dimple. This pattern is called in-line pattern. In the second figure, the jets impinge between the dimples. This pattern is called staggered pattern. All dimples are of 1.27 cm diameter. Two different dimple depths of 0.3175 and 0.15875 cm are used to study the effect of dimple depth. The dimple size was based on the assumption that the jet would impinge completely within the dimple. The depth was based on earlier studies that suggested a dimple diameter to depth ratio ranging between 0.125 and 0.25. A thermocouple is placed at inlet of the pressure channel to measure the local temperature of the heated air. The transient thermocouple output is digitized during the test using the InstruNet 8-Channel A/D system.

3. Methodology and procedure

The air mass flow rate is set for the required jet average Reynolds number condition, and then heated through the in-line air heater. The temperature at the exit of the heater is set based on some qualification tests to produce acceptable liquid crystal color change times during the transient test. The heated air is routed away from the test section. The temperature measurement system and the image processing system are set to initiate data measurement at the same instant as the diverter valve is flipped. The test section is ready for running when the air is heated to the steady required temperature. The diverter valve is flipped to let the hot air into the test section. The thermochromic liquid crystal coating is heated by the hot air and changes color when it reaches its display color range. Liquid crystal color temperatures are pre-set and are calibrated under lab lighting conditions. The liquid crystal used in this study has a narrow band with the initial red color appearing at 35.1 °C, then green color appearance at 35.4 °C, and finally blue color at 35.9 °C. The total band is 1 °C. The image processing system divides the test section into tiny pixel locations and monitors each location individually for color changes. The test section in this study was divided into 400×200 pixels. The reference point in this study is set as the appearance of green color during the transient. This indicates that the image processing system will provide time of color changes at every pixel when it reaches 35.4 °C. The test duration is typically a maximum of 150 s. The air temperature is set such that the times of color changes at all pixels are between 10–150 s. It takes typically 3–5 s for the flow to achieve a steady-state condition. However the temperature response is relatively slower so the mainstream

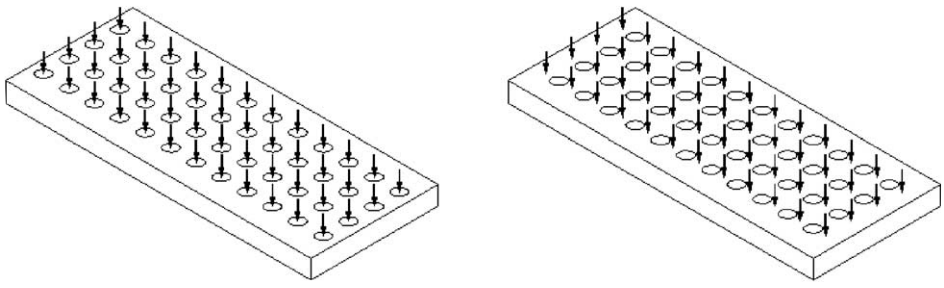

Fig. 3. Dimple configurations (in-line and staggered).

temperature response is taken into consideration during the calculation of the local heat transfer coefficient. The reason for this is that the test section wall should not violate the semi-infinite solid assumption.

The test section is made of plexiglass so that a 1-D semi-infinite solid assumption can be applied on the test section wall (Huang et al., 1998). The time-step changes are then included into the equation to obtain a function of the form

$$T_w - T_i = \sum_{j=1}^{N} \{1 - \exp\left[\frac{h^2\alpha(t-\tau_j)}{k^2}\right] \times \operatorname{erfc}\left[\frac{h\sqrt{\alpha(t-\tau_j)}}{k}\right]\} \left[\Delta T_{m,(j,j-1)}\right], \quad (1)$$

where $\Delta T_{m,(j,j-1)}$ and τ_j are the inlet air temperature and time-step changes interpolated from the digitized temperature output. The equation is solved at every pixel location to obtain the local heat transfer coefficient, h. Huang et al. (1998) used a similar approach. The average experimental uncertainty based on the methodology of Kline and McClintock (1953) is on the order of ±6.5%. The thickness of the plexiglass plate underneath the dimple is sufficient to satisfy the semi-infinite solid assumption. A simple analysis shows that the temperature penetration through the plexiglass plate does not occur till about 300 s for a 1.27 cm thick plexiglass plate. The only regions of higher uncertainty are the dimple edges where the edges have been rounded to reduce the 2-D conduction effects.

4. Results and discussion

All the results are presented in terms of Nusselt number ratios. The local Nusselt number with dimples is normalized using the Nusselt number without dimples. The smooth results were repeated and the results thus obtained were in good agreement with the results in the same rig presented by Huang et al. (1998). Two configurations of dimples are tested as shown in Fig. 3. Also, for each dimple configuration, the effect of dimple depth is also presented.

Huang et al. (1998) presented flow measurements inside the impingement channel. They measured pressure drop across the impingement holes using static pressure taps. Fig. 4 shows the local individual jet flow through each of the 12 rows and the cross-flow distributions for the impingement channel. The jet mass flow rate through each row of holes is presented along the cross-flow streamwise direction. The jet mass flow distribution is even through the channel with exception for the first two rows near the inlet. The axial velocity of the flow near the inlet may be too high to ensure that equivalent flow enters through the initial rows. The

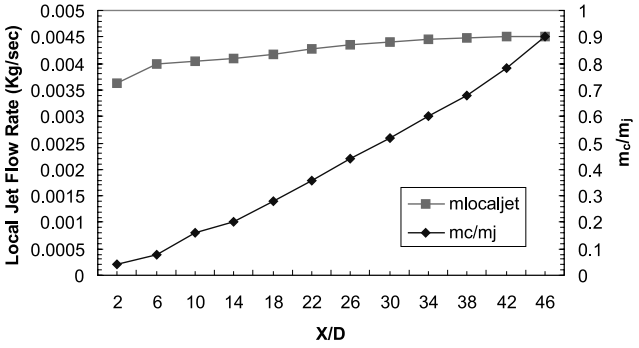

Fig. 4. Flow distributions in the test section with jet impingement.

cross-flow increases from inlet side of the impingement channel to the exit. As flow enters the impingement channel through each downstream row, cross-flow increases. This cross-flow pushes the downstream jets away from the surface.

Fig. 5 presents the detailed Nusselt number (Nu) distributions for in-line and staggered dimple configurations for $Re = 9800$. The dimple depth is 0.3175 cm. The dimple locations are indicated on the contour plots. The jets are in line with the dimple location for the in-line case. At the inlet side, the jets impinge directly inside the dimple as seen in the detailed distributions. The Nusselt numbers along the column of jets are higher and lower between the jets in each row. The dimples appear to produce little effect on the jet impingement for the

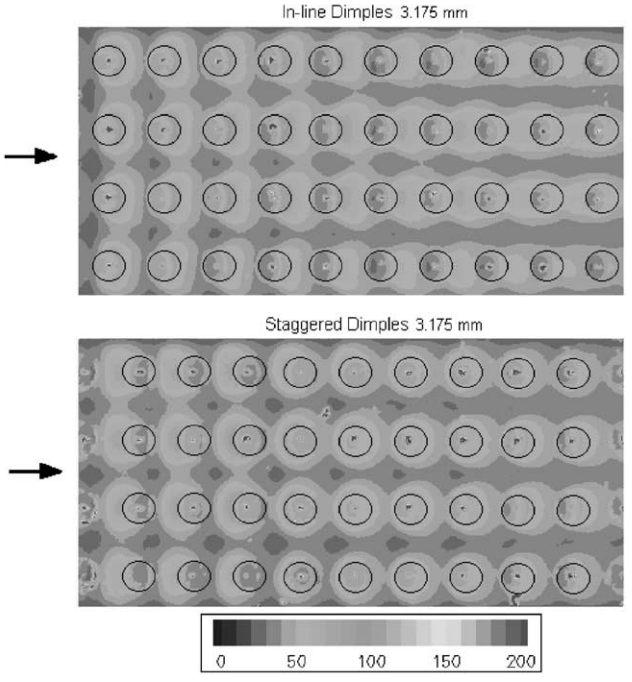

Fig. 5. Detailed Nusselt number distributions for $Re = 9800$ with in-line and staggered dimples.

initial rows of jets. Further downstream as the cross-flow develops, the jets are pushed towards the exit and impinge between the dimples enhancing the region between the dimples. The heat transfer coefficients inside the dimples are reduced due to flow separation and reattachment phenomena. The high heat transfer region produced by the jets moves from inside the dimple location near entrance to downstream of the dimple location near exit. The cross-flow effect is distinct.

For the staggered dimple configuration, the jets near entrance impinge between the dimples enhancing heat transfer coefficients. The heat transfer coefficients between the jet impingement around and inside the dimples are reduced. Further downstream, the jet impingement location gets shifted to inside the dimple with stronger cross-flow effect. In this case also, the cross-flow effect is distinct. The advantage of using dimples on a jet impingement target surface can only be determined by comparing the local Nusselt number distributions for a surface with dimples to a surface without dimples. All the spanwise results are shown as a ratio of the Nusselt number with dimples (Nu) normalized by the local Nusselt number without dimples (Nu_0).

Fig. 6 shows the effect of jet average Reynolds number on spanwise-averaged Nusselt number ratio (Nu/Nu_0) for the in-line configurations and different depths. The presence of dimples on the target surface produces lower heat transfer coefficients than on a non-dimpled surface. For the in-line dimples geometry, the Nusselt number ratios increase from inlet to exit as cross-flow becomes stronger. It appears that the heat transfer coefficient is significantly reduces for pure impingement which is the case at small X/D and increases downstream as cross-flow increases. This indicates that heat transfer coefficient enhancement occurs when the flow assumes a channel flow situation. If the channel is extended further downstream without impingement, heat transfer coefficient enhancement would occur due to the flow becoming a channel type flow. This is consistent with the findings of the studies on dimple effects in channel flows (Chyu et al., 1997; Moon et al., 1999). There is a decrease in the Nusselt number ratio values from $Re = 4800$ to $Re = 9800$ and then a slight increase with increase in Reynolds number form $Re = 9800$ to $Re = 14\,800$ for both in-line and staggered dimples. Fig. 7 shows the effect of jet average Reynolds number for the shallow (0.1575 cm) dimple configurations. The trends are identical for the shallow dimples.

Fig. 8 presents the effect of dimple configuration for both dimple depths at $Re = 9800$. It appears that in-line geometry produces slightly higher Nusselt number ratios than the staggered pattern for both dimple depths. The effect of configuration is strongly evident in the region $X/D > 25$ where the in-line configuration produces much higher Nusselt numbers than the staggered con-

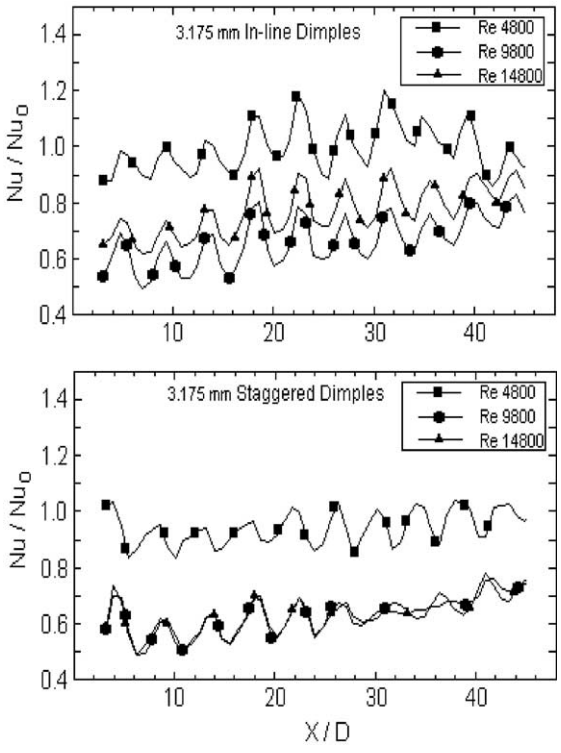

Fig. 6. Effect of jet average Reynolds number on spanwise-averaged Nusselt number ratio distributions for the deep dimple configurations.

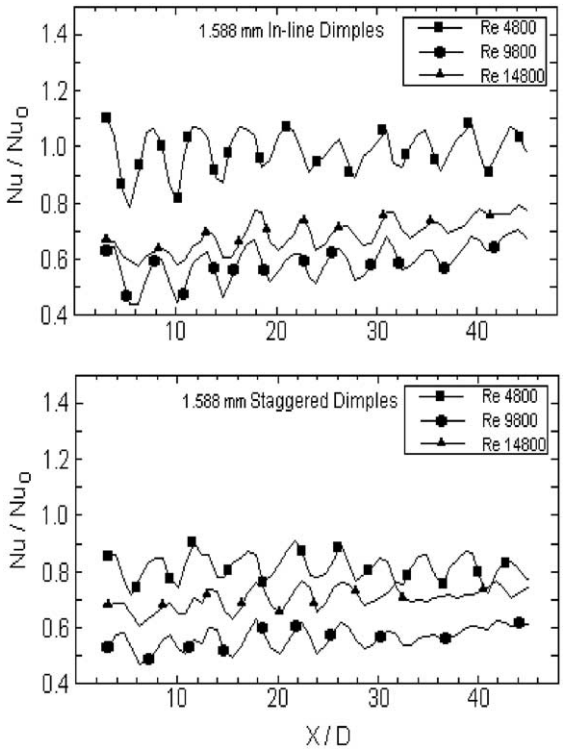

Fig. 7. Effect of jet average Reynolds number on spanwise-averaged Nusselt number ratio distributions for the shallow dimple configurations.

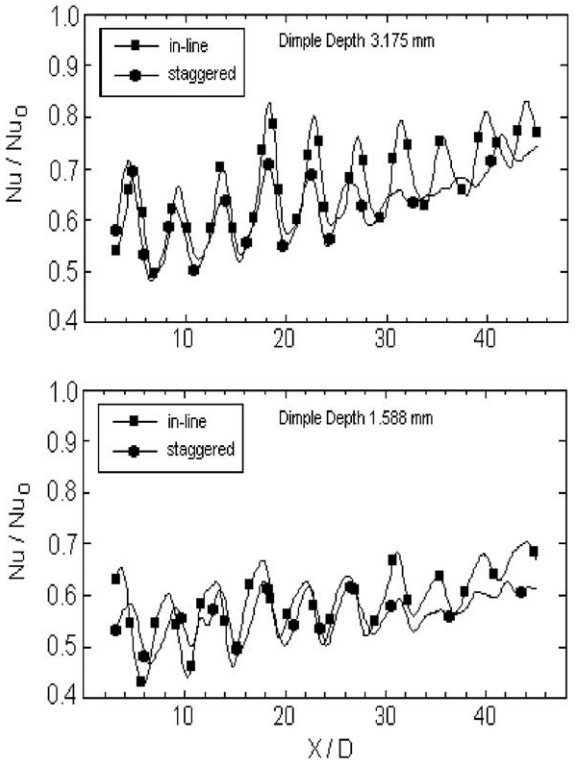

Fig. 8. Effect of dimple configuration on spanwise Nusselt number ratio distributions for both dimple depths at $Re = 9800$.

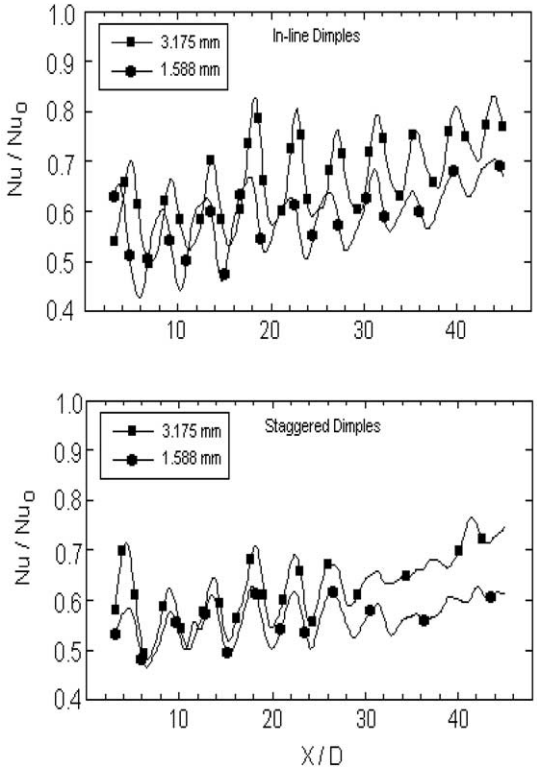

Fig. 9. Effect of dimple depth on spanwise Nusselt number ratio distributions for both dimple configurations at $Re = 9800$.

figuration. This was pointed out in the discussion on the detailed distributions. At larger X/D locations, the jets impinge inside the dimples for the staggered array causing significant reductions in the local heat transfer coefficient due to bursting of the jets. The peaks and the valleys due to jet impingement are reduced due to the breakdown of jet structure for the cross-flow affected weaker jets especially for the shallow dimples.

Fig. 9 presents the effect of dimple depth for both dimple configurations at $Re = 9800$. It is clearly evident that the deeper dimples provide higher heat transfer coefficients for both configurations. The shallow dimples may be producing stronger bursts resulting in the reduced jet impingement compared to a deeper dimple where the burst is entrained inside the dimple and does not affect the impingement. The results show a need for stronger understanding of the fluid mechanics of the jets after impingement in and around dimples. It is difficult to provide a detailed explanation on the phenomena purely on the basis of surface heat transfer distributions. However, the results provide some clear understanding of the impact of dimples in producing lower or almost negligible enhancement when combined with a high heat transfer enhancement technique such as impingement. This finding is clearly the most important result of this study.

Fig. 10 presents the overall area-averaged Nusselt number ratio ($\overline{\overline{Nu}}/\overline{\overline{Nu}}_0$). The local Nusselt number values at every location on the detailed distributions are taken and area averaged to determine the overall Nusselt number ratio. The dimpled surface has a larger surface area exposed to the jet impingement than the flat target surface. However, this has not been considered in presenting the overall averaged comparisons. The results from the present study are based on the projected area of the dimple and not the true surface area of the dimples. The results for each dimple configuration are plotted against average jet Reynolds number. Results show that the ratio values are close to 1.0 for a low

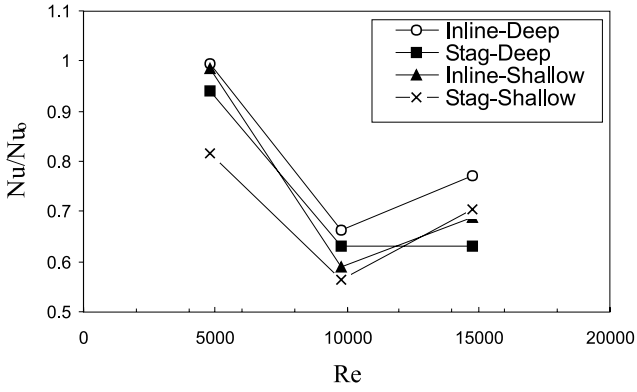

Fig. 10. Comparison of overall-averaged Nusselt number ratio trends versus jet Reynolds number for all the tested configurations.

Reynolds number of 4800, then decreases to values around 0.6 for $Re = 9800$ and then increase to around 0.7 for $Re = 14\,800$. The trend is the same for all the cases. The in-line dimple configuration with deeper dimples provides the highest overall heat transfer ratio of the four-tested configurations. The staggered dimple configuration with shallow dimples provides the lowest overall heat transfer ratio.

5. Conclusions

Heat transfer measurements are presented for a jet impingement target plate with dimples. Two-dimple configurations, in-line and staggered with respect to the jet impingement hole position, are compared. The effect of dimple depth has also been investigated. Results indicate that the presence of dimples produces lower heat transfer coefficients on the target surface compared to the plain target surface. Heat transfer coefficients increase as cross-flow increases confirming the enhancement of heat transfer coefficients for channel flow behavior. The jet structures on impingement in and around dimples seem to be affected by the bursting phenomena of the flow inside the dimples resulting in reduced impingement effect. Unlike in channel flows, the bursting phenomenon produces local turbulence, flow separation and reattachment, the bursting phenomenon with jet impingement breaks up the impingement core. The present pattern of impingement inside and between dimples along axial directions may not be the optimum pattern for heat transfer enhancement.

Acknowledgements

The authors wish to acknowledge the support from the project funded by Louisiana Board of Regents through the NASA-LaSPACE REA under contract NASA/LEQSF (1996-2001). The program manager is Dr. John Wefel. The authors also wish to acknowledge Prof. J. C. Han of Texas A&M University for providing the test rig and providing some insightful comments on this work.

References

Behbahani, A.I., Goldstein, R.J., 1983. Local heat transfer to staggered arrays of impinging circular air jets. ASME J. Eng. Power 105, 354–360.

Chupp, R.E., Helms, H.E., McFadden, P.W., Brown, T.R., 1969. Evaluation of internal heat transfer coefficients for impingement cooled turbine blades. J. Aircraft 6, 203–208, also AIAA Paper 68-564, 1968.

Chyu, M.K., Yu, Y., Ding, H., 1997. Concavity enhanced heat transfer in an internal cooling passage. ASME Paper no. 97-GT-437.

Downs, S.J., James, E.H., 1987. Jet impingement heat transfer – a literature survey. ASME Paper no. 87-HT-35.

Florschuetz, L.W., Truman, C.R., Metzger, D.E., 1981. Streamwise flow and heat transfer distribution for jet array impingement with crossflow. ASME J. Heat Transfer 103, 337–342.

Florschuetz, L.W., Metzger, D.E., Su, C.C., Isoda, Y., Tseng, H.H., 1984. Heat transfer characteristics for jet array impingement with initial crossflow. ASME J. Heat Transfer 106, 34–41.

Huang, Y., Ekkad, S.V., Han, J.C., 1998. Local heat transfer coefficient distribution under an array of impinging jets using a transient liquid crystal technique. AIAA J. Thermal Heat Transfer 12, 73–79.

Huber, A.M., Viskanta, R., 1994a. Effect of jet–jet spacing on convective heat transfer to confined, impinging arrays of axisymmetric air jets. Int. J. Heat Mass Transfer 37, 2859–2869.

Huber, A.M., Viskanta, R., 1994b. Comparison of convective heat transfer to perimeter and center jet in a confined, impinging array of axisymmetric air jets. Int. J. Heat Mass Transfer 37, 3025–3030.

Kercher, D.M., Tabakoff, W., 1970. Heat transfer by a square array of round air jets impinging perpendicular to a flat surface including the effect of spent air. ASME J. Eng. Power 92, 73–82.

Kline, S.J., McClintock, F.A., 1953. Describing uncertainties in single sample experiments. Mech. Eng. 175, 3–8.

Lin, Y.L., Shih, T.I.-P., Chyu, M.K., 1999. Computations of flow and heat transfer in a channel with rows of hemispherical cavities. ASME Paper no. 99-GT-253.

Moon, H.K., O'Connnell, T., Glezer, B., 1999. Channel height effect on heat transfer and friction in a dimpled passage. ASME Paper no. 99-GT-163.

Schukin, A.V., Kozlov, A.P., Agachev, 1995. Study and application of hemispherical cavities for surface heat transfer augmentation. ASME Paper no. 95-GT-59.

Van Treuren, K.W., Wang, Z., Ireland, P.T., Jones, T.V., 1994. Detailed measurements of local heat transfer coefficient and adiabatic wall temperature beneath an array of impingement jets. ASME J. Turbomach. 116, 369–374.

Viskanta, R., 1993. Heat transfer to impinging isothermal gas and flame jets. Exp. Thermal Fluid Sci. 6, 113–134.